Punching shear in prestressed concrete deck slabs
a comprehensive study

Amir, Sana; van der Veen, Cor; Walraven, Joost C.; de Boer, Ane

DOI
10.14359/51738765

Publication date
2023

Document Version
Final published version

Published in
Punching Shear of Concrete Slabs

PUNCHING SHEAR IN PRESTRESSED CONCRETE DECK SLABS: A COMPREHENSIVE STUDY

Sana Amir, Cor van der Veen, Joost C. Walraven and Ane de Boer

Synopsis: A large number of bridges in the Netherlands have transversely post tensioned deck slabs cast in-situ between flanges of precast girders and were found to be critical in shear when evaluated by Eurocode 2. To investigate the bearing (punching shear) capacity of such bridges, a 1:2 scale bridge model was constructed in the laboratory and static tests were performed by varying the transverse prestressing level (TPL). A 3D solid, 1:2 scale model of the real bridge, similar to the experimental model, was developed in the finite element software DIANA and several nonlinear analyses were carried out. It was observed that the experimental and numerical ultimate load carrying capacity was much higher than predicted by the governing codes due to lack of consideration of compressive membrane action (CMA). In order to incorporate CMA in the Model Code 2010 (*fib* 2012) punching shear provisions for prestressed slabs, numerical and theoretical approaches were combined. As a result, sufficient factor of safety was observed when the real bridge design capacity was compared with the design wheel load of Eurocode 1. It was concluded that the existing bridges still had sufficient residual bearing capacity with no problems of serviceability and structural safety.

Keywords: Concrete, Deck slab, Punching shear, Transverse prestressing, Wheel loads, Compressive Membrane Action.

INTRODUCTION

Background

The safety of existing, old structures is a crucial subject all over the world. In the Netherlands, a large number of transversely prestressed bridge decks that were built 5-6 decades ago need to be investigated for their structural safety under the actual (increased) traffic loads. This research is an attempt to investigate the bearing (punching shear) capacity of such bridge decks under concentrated loads (wheel loads). The safety criteria against bearing capacity is not satisfied for these bridges if evaluated by Eurocode 2 "Concrete structures" (EN 1992-1-1:2005).[1] However, since the bridge decks are laterally restrained by the flanges of the supporting girders, it is expected that compressive membrane action (CMA) exists in such deck slabs. Therefore, the transverse prestressing of the deck slab in combination with CMA may enhance the bearing capacity, making thinner deck slabs possible with no problems of serviceability and structural safety.

In order to investigate the research problem experimentally, laboratory tests on a 1:2 scale bridge model of a real bridge in the Netherlands have been carried out.[2] The model bridge consisted of a thin, transversely prestressed concrete deck cast in-situ between the flanges of long prestressed concrete girders (**Figure 1**). The effect of various parameters, like the transverse prestressing level (TPL), the type and position of the load(s), the inclination of the joint (interface), the size of the loading plate etc., on the bearing capacity were also studied.[3]

Figure 1 – 1:2 scaled model of the bridge in the laboratory

As part of the numerical investigation, a 3D solid, 1:2 scale model of the real bridge (**Figure 2**), similar to the experimental model, was developed in the finite element software TNO DIANA (FX+ 9.4.4)[4] and several nonlinear analyses were carried out whose details can be found in Amir[5].

A comparison with the experimental results was made proving that satisfactory results were obtained that validated the finite element model.[6] The normal forces arising from compressive membrane action were determined with the help of composed elements.[4] A detailed parametric study was also carried out involving numerical modeling parameters, like the mesh size, displacement-load step size etc., and the material and geometrical parameters, similar to the experimental parametric study.[7] In addition to that, the size effect[8] was studied by carrying out a nonlinear analysis on a 3D solid model of the real bridge.

This paper summarizes the experimental and numerical research carried out on the model bridge deck, describes the approach used to incorporate compressive membrane action in the punching shear provisions of the Model Code 2010 (*fib* 2012)[9] and then investigates the structural safety of the real bridge against the design wheel (traffic) loads. Using this approach, an average safety factor of 3.5 is obtained when the projected model bridge design capacity and the real bridge design capacity were compared with the design wheel load of Load model 1, EN 1991-2:2002[10].

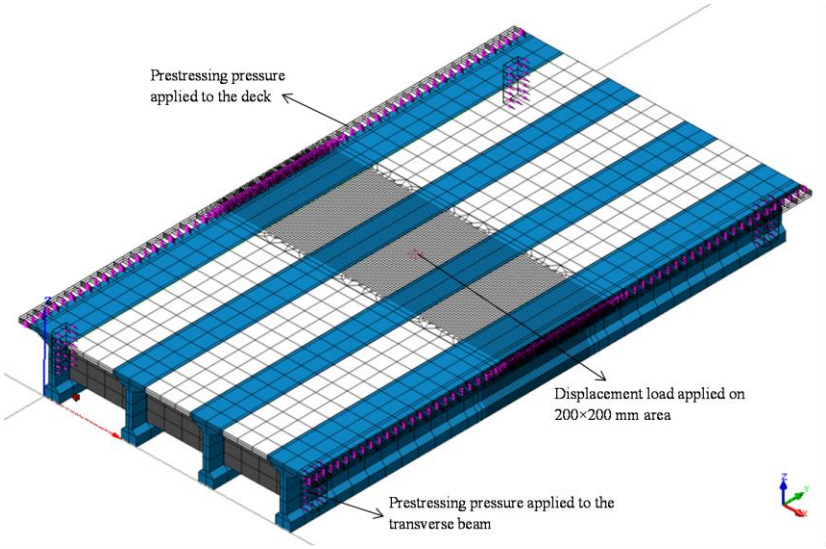

Figure 2 – 3D solid Finite Element 1:2 scale model of the real bridge

Compressive Membrane Action

Hewitt and Batchelor describe compressive membrane action (CMA) as a phenomenon that occurs in laterally restrained slabs. Under the action of the load, changes of geometry cause the slab edges to tend to move outward and to react against the stiff boundary elements as shown in **Figure 3**[12]. This phenomenon cannot occur in slabs with the same strength in tension and compression. Moreover, the presence of reinforcement is not necessary. CMA leads to an increase in the bearing capacity of the slab and it fails at a load much higher than predicted by the standard yield line theory. The increase is seen in both the flexural and the punching shear capacity of a restrained slab, however, it is the punching shear that becomes the governing mode of failure.[13-17] It is quite tedious to quantify membrane action, so some codes [18,19] have included CMA empirically in their design provisions, however, for reinforced concrete decks only. To date, none of the existing codes have incorporated compressive membrane action in the design or capacity assessment provisions for prestressed slabs or deck slabs. In this research, an attempt is made to develop a user-friendly technique to estimate the compressive membrane action and calculate the punching shear capacity including the positive effect of the membrane forces.

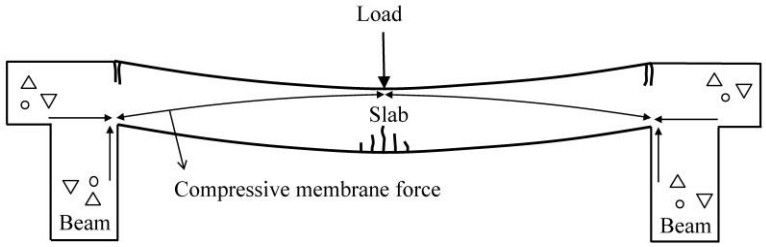

Figure 3 – Compressive membrane action in a reinforced concrete bridge deck slab[12]

RESEARCH SIGNIFICANCE

This research investigates the critical problem of determining the bearing (punching shear) capacity of existing transversely prestressed concrete bridge decks by experimental, numerical and theoretical approaches. By combining the results of finite element analyses and Model Code 2010[9] punching shear provisions, a new method that incorporates compressive membrane action and predicts bearing capacity of laterally restrained deck slabs more accurately has been developed. Results showed an adequate safety margin against the Eurocode design wheel load

leading to the conclusion that these old bridges still have sufficient residual bearing (punching shear) capacity and significant savings in cost can be made if compressive membrane action is considered in the analysis.

EXPERIMENTAL INVESTIGATION

Real bridge

For this research, the bridge selected for investigation consisted of a number of 50 m (164 ft) approach spans having 200 mm (8 in.) thick post-tensioned deck slab panels cast in-situ between the flanges of simply supported, post-tensioned girders (3000 mm (120 in.) high and spaced at 3600 mm (144 in.) c/c). At the time of casting, the bridge deck had normal strength concrete but at present the strength is much higher due to continuous hydration over the years. Minimal ordinary reinforcement is provided. The usual spacing of the prestressing tendons in the slab is around 650 mm (26 in) c/c with the exception of a few places where it is 800 mm (32 in.) c/c. An inclined indented interface is provided between the girder flange-deck slab joint to generate sufficient shear capacity. The deck slab has transversely prestressed end transverse beams at the supports. Diaphragms are provided at 1/3rd and 2/3rd of the span. The real bridge is described in detail in Amir.[5]

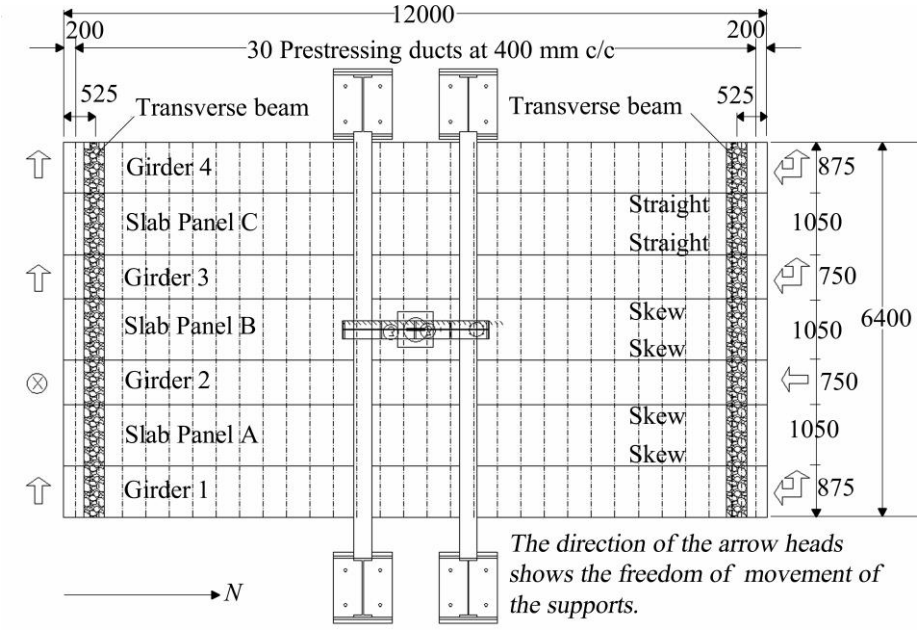

(a)

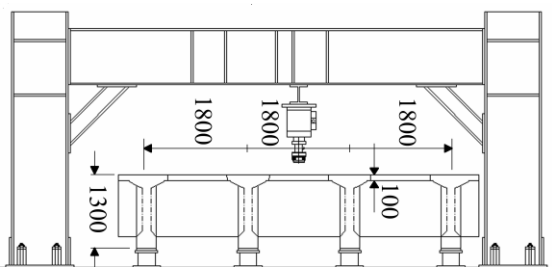

(b)

Figure 4 – An overview of the laboratory test-setup: a) Top view; b) Transverse view.
Note: All dimensions are in mm; 1 mm = 0.04 in.

Prototype of the bridge

Since the laboratory space was limited, a 1:2 scale was used to design the prototype and it was ensured that failure would occur in the deck slab and not the girders. **Figure 4(a) and 4(b)** show the test specimen representing the prototype bridge. The deck had a width of 6.4 m (21 ft) and height of 12 m (39.36 ft). The main span was 10.95 m (35.92 ft) long with a cantilever of 525 mm (21 in.) at each end. Four precast concrete girders, having a height of 1300 mm (52 in.), were spaced at 1800 mm (972 in.) c/c. The three deck slab panels having a thickness of 100 mm (4 in.) were cast in-situ and post-tensioned in the transverse direction with a clear span of 1050 mm (42 in.). Two post-tensioned transverse beams, 810×350 mm (32.4×14 in.), were provided at 525 mm (21 in.) from each end of the bridge deck. The design of the prototype was based on lower bound criteria.[5]

Components of the test-setup

Four precast-prestressed girders were made by Spanbeton, the Netherlands and transported to the laboratory. A typical girder is shown in **Figure 5(a)**. An extended width of 125 mm (5 in.) was provided at the exterior flanges [**Figure 5(b)**] to make sure that the prestressing and the confining effect was introduced adequately. The location of straight and inclined (1:20) interfaces between the deck slab panel and the girder flange are shown in plan in **Figure 4(b)**. The indented interface (classified as smooth according to Eurocode 2[1], **Figure 5(d)** between the slab and the girder had an inclination of 1:20 [**Fig 5(c)**]. The transverse beams, 810×350 mm (32.4×14 in.), were cast at 525 mm (21 in.) from each end of the bridge deck [**Figure 4(b)**]. Both the deck slab and the transverse beams had similar transverse prestressing steel consisting of 15 mm (0.6 in.) Φ unbonded bars and post-tensioned to the desired level. The prestress level in each bar was monitored in order to record any losses over time. Both the deck slab and transverse beams were provided with nominal, regular steel reinforcement. The material properties are given in **Table 1**.

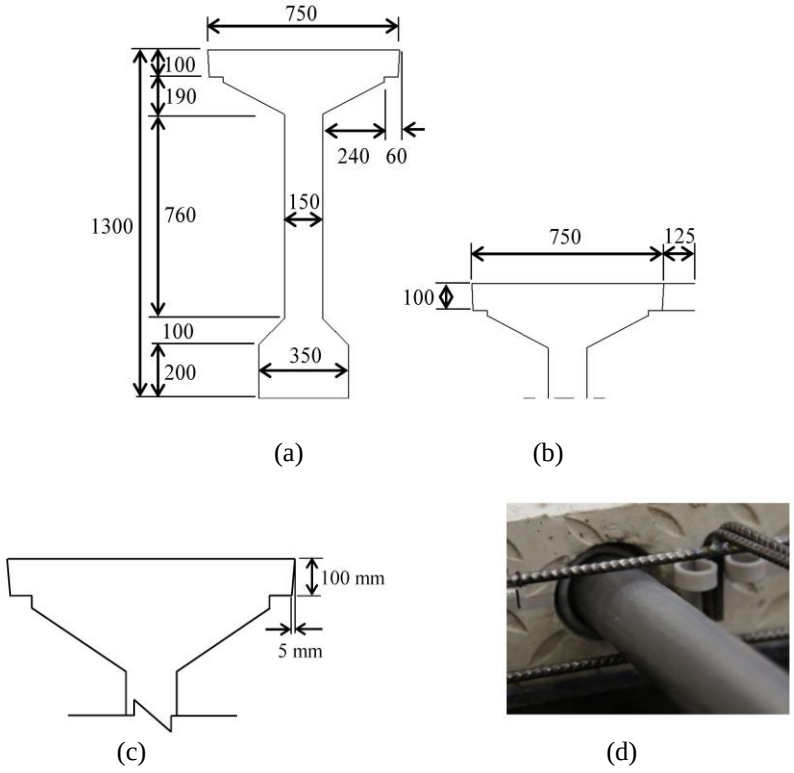

Figure 5 – a) Model bridge interior girder; b) Model bridge exterior girder with an extended flange width of 125 mm; c) Skewness of the girder flange interface; d) Roughness-Ruukki DIN 59220 teardrop pattern used to produce the indented interface between the girder flange and the deck slab. The picture is taken before casting of concrete in the deck slab.
Note: All dimensions in mm; 1 mm = 0.04 in

Table 1 – Material properties of various component of the model bridge

Component	Material	Property	Value
Deck Slab and Transverse Beams	Concrete	Mean compressive cylinder strength, f_{cm} [MPa]	65
		Mean tensile strength, f_{ctm} [MPa])	5.4
		Modulus of elasticity, E_{cm} - EC2 [GPa]	39
	Prestressing Steel	Characteristic tensile strength, f_{pk} [MPa]	1100
		Characteristic 0.1% proof stress, $f_{p0.1k}$ [MPa]	900
		Modulus of elasticity, E_p [GPa]	205
	Ordinary Steel	Mean yield strength, f_{sy} [MPa]	525
		Mean ultimate tensile strength, f_{su} [MPa]	580
		Modulus of elasticity, E_s [GPa]	200
Girders	Concrete	Mean compressive cylinder strength f_{cm} [MPa]	75
		Mean tensile strength, f_{ctm} [MPa]	6.3
		Modulus of elasticity, E_{cm} - EC2 [GPa]	40

Note: EC2 = Eurocode 2; 1 MPa = 145 psi.

Load application

A concentrated load simulating a wheel print load was applied by the hydraulic actuator attached to an overhead reaction frame bolted to the floor (**Figure 1)**. In all the tests, the load[1] (see **Figure 6** for the load configuration [EN 1991-2:2002[10]]) was applied through a 200×200 mm (8×8 in.), 8 mm (0.32 in.) thick rubber bonded to two 200×200×20 mm (8×8×0.8 in.) steel plates.

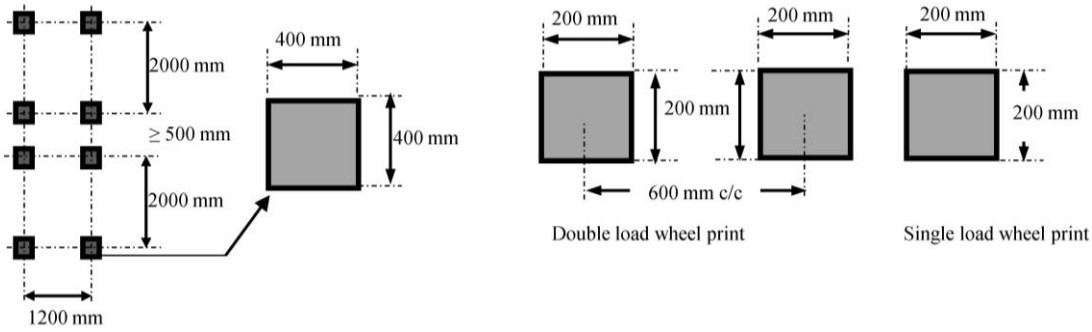

(a) (b)

Figure 6 – a) Eurocode load configuration and wheel print (Load model 1, EN 1991-2:2002); b) Single and double load wheel print according to the Eurocode scaled down to 1:2. Note: 1 mm = 0.04 in

Test parameters

Table 2 shows the test configuration and related parameters. **Figure 7** shows the location of the loads on the deck slab panels as well as sequence of the tests. Both exterior (A and C) and interior (B) deck slab panels (**Figure 7**) were tested at several locations along the length of the deck.

Four types of tests were performed.

- Single wheel print load acting at midspan of deck slab panel, P1M.
- Single wheel print load acting close to the girder flange-deck slab interface/joint, P1J.
- Double wheel print loads at 600 mm (24 in.) c/c acting at midspan of deck slab panel, P2M.

[1] The concentrated load was according to Eurocode 1 Load model 1[10] and the wheel print of 400×400 mm (16 ×16 in.) was scaled down according to 1:2. The double load consisted of two point loads placed at a distance of 0.6 m (2 ft) c/c, scaled down from 1.20 m (4 ft) c/c (**Fig. 6**).

- Double wheel print loads at 600 mm (24 in.) c/c acting close to the girder flange-deck slab interface/joint, P2J.

Table 2 – Testing Configuration

#	Test	Panel	Load type	TPL	Joint	Designation
				[MPa]		
1	BB1	C-Midspan	Single (BD)	2.5	Straight	C-P1M-ST
2	BB2	A-Midspan	Single (BD)	2.5	Skewed	A-P1M-SK
3	BB3	A-Interface	Single (BD)	2.5	Skewed	A-P1J-SK
4	BB4	C-Interface	Single (BD)	2.5	Straight	C-P1J-ST
5	BB5	C-Midspan	Double (BD)	2.5	Straight	C-P2M-ST
6	BB6	A-Interface	Double (BD)	2.5	Skewed	A-P2J-SK
7	BB7	C-Midspan	Single (BD)	2.5	Straight	C-P1M-ST
8	BB8	C-Midspan	Single (BD)	1.25	Straight	C-P1M-ST
9	BB9	A-Midspan	Single (BD)	1.25	Skewed	A-P1M-SK
10	BB10	A-Interface	Single (BD)	1.25	Skewed	A-P1J-SK
11	BB11	C-Midspan	Double (BD)	1.25	Straight	C-P2M-ST
12	BB12	A-Interface	Double (BD)	1.25	Skewed	A-P2J-SK
13	BB13	C-Midspan	Single (AD)	1.25	Straight	C-P1M-ST
14	BB14	C-Interface	Single (AD)	1.25	Straight	A-P1J-ST
15	BB15	A-Midspan	Single (AD)	1.25	Skewed	A-P1M-SK
16	BB16	B-Midspan	Double (BD)	2.5	Skewed	B-P2M-SK
17	BB19[a]	B- Midspan	Single (BD)	2.5	Skewed	B-P1M-SK
18	BB21	B-Midspan	Single (BD)	0.5	Skewed	B-P1M-SK
19	BB22	B-Midspan	Single (BD)	0.5	Skewed	B-P1M-SK

Note: [a] = SLP (115×150mm [4.6×6 in.]); TPL = Transverse prestressing level; AD = above duct; BD = In-between two ducts; ST = Straight joint; SK = Skewed joint; P1M = Single wheel print load acting at midspan of deck slab panel; P1J= Single wheel print load acting close to the girder flange-slab interface/joint; P2M = Double wheel print load acting at midspan of deck slab panel; P2J= Double wheel print load acting close to the girder flange-slab interface/joint; 1 MPa = 145 psi; 1 mm = 0.04 in.

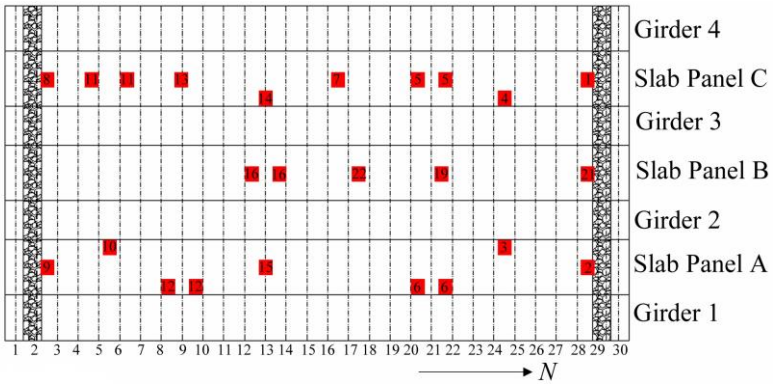

Figure 7 – Deck slab load locations (numbered according to testing sequence). Duct locations are also shown.

For most of the interface (J) tests, the load was applied at 200 mm (8 in.) from the interface (c/c) with the exception of test BB3 and BB4, where the center of the loading plate was at 110 mm (4.4 in.) from the interface. Sixteen out of nineteen tests were performed by placing the center of the loading plate in-between the transverse prestressing ducts (BD). The remaining three tests were carried out with the load just above a duct (AD) as it has been shown in the literature[20] that testing directly above a duct gives a higher capacity than testing in-between the ducts. The size of the

loading plate was 200×200 mm (8×8 in.) in all the tests with the exception of test BB19 where a 115×150 mm[2] (4.6×6 in.) small loading plate (SLP) was used. The transverse prestressing levels (TPLs) ranged from 0.5 MPa (72.5 psi), 1.25 MPa (181.25 psi) and 2.5 MPa (362.5 psi). The punching shear capacity obtained from the experiments is given in **Table 3**. The detailed test reports are collected in Stevin Report No. 25.5.13-06.[21]

Table 3 – Summary of Test Results

Test BB.	TPL	Designation	FMODE	P_T	P_{FEA}	P_T/P_{FEA}
	[MPa]			[kN]	[kN]	
1.	2.5	C-P1M	BP	348.7	302.3	1.15
2.	2.5	A-P1M	BP	321.4	302.3	1.06
3.	2.5	A-P1J	BP	441.6	429.9	1.03
4.	2.5	C-P1J	BP	472.3	429.9	1.10
5.	2.5	C-P2M	FP	490.4	529.9	0.93
6.	2.5	A-P2J	BP	576.8	537.0	1.07
7.	2.5	C-P1M	BP	345.9	302.3	1.14
8.	1.25	C-P1M	BP	284.5	271.4	1.05
9	1.25	A-P1M	BP	258.2	271.4	0.95
10.	1.25	A-P1J	BP	340.3	300.7	1.13
11.	1.25	C-P2M	FP	377.9	453.4	0.83
12.	1.25	A-P2J	BP	373.7	454.9	0.82
13.	1.25	C-P1M (AD)	FP	322.9	363.1	0.89
14.	1.25	A-P1M (AD)	BP	295.9	294.0	1.01
15.	1.25	A-P1M (AD)	FP	359.7	363.1	0.99
16.	2.5	B-P2M	FP	553.4	592.7	0.93
19.	2.5	B-P1M (SLP)	BP	317.8	306.0	1.04
21.	0.5	A-P1M	FP	243.8	274.6	0.89
22.	0.5	A-P1M	FP	257.5	274.6	0.94
			Mean			**1.00**
			Standard deviation			**0.10**
			Coefficient of variation (COV)			**0.10**

Note: P_T = Test failure load; P_{FEA} = Finite Element Analysis failure load; AD= Above duct; SLP: Small loading plate; FMODE = Test failure mode; BP = Brittle punching; FP = Flexural punching; 1 MPa = 145 psi; 1 kN = 0.225 kip; 1 mm = 0.04 in.

NUMERICAL ANALYSIS

Prototype bridge deck

For the numerical analysis, a 3D solid finite element model (2ELEM) of the prototype bridge deck was made in the FEA software package TNO DIANA (FX+ 9.4.4)[4] conforming to recommendations of RTD 1016:2012.[22] The general model is shown in **Figure 2**. Nonlinear analyses were performed for the deck slab panels; however, the girders and transverse beams were analyzed linearly (no reinforcement was provided) since it was known from the experiments that they do not show any nonlinear behavior. For cases where the load was applied very close to the interface (110 mm (4.4 in.) c/c distance between the loading plate and the interface in tests BB3 and BB4), the nearby flange of the loaded interface was analyzed nonlinearly since the linearity of the girders led to an unrealistic high capacity in such cases. The mesh size was finer in the middle zone of the bridge deck where the load was applied as compared to the rest of the bridge deck (**Figure 2**).

Structural modeling and nonlinear material properties

The bridge model consisted of 3D solid elements (CHX60 and CTP45) and a layer of composed elements (CQ8CM) in the fine mesh area (**Figure 8**) to calculate compressive membrane forces (N_{xx}, the in-plane forces). The regular

[2] The 115×150 mm (4.6×6 in.) size is related to the super single wheel print according to the "Richtlinie zur Nachrechnung von Straßenbrücken im Bestand (Nachrechnungsrichtlinie)", Bundesministerium für Verkehr, Bau und Stadtentwicklung, Abteilung Straßenbau, Germany, 05/2011.

steel reinforcement was modeled as an embedded grid based on the actual reinforcement ratio. **Table 1** shows the the material properties of the linearly modeled structural components (girders and transverse beams). A smeared cracking "Total strain crack rotating model" was selected for the nonlinear analysis. An elastic-perfectly plastic model, CONSTA, was used for the concrete behavior in compression, whereas, an exponential softening curve, HORDIJK[23], was used for the concrete behavior in tension. A fracture energy G_f of 0.15 N/mm (0.86 lb/in) was assumed for the deck slab concrete. The poisson ratio, ν, for all the concrete components, was taken as 0.2. For the embedded grid reinforcement, the von Mises plasticity criterion was used with a poisson ratio of 0.3.

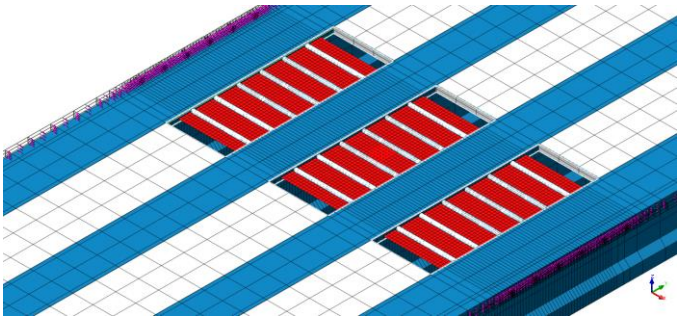

Figure 8 – Layer of composed elements (shown in red) and prestressing ducts provided only in the central region having a mesh size finer than the rest of the 3D solid model.

Applied loads and support constraints

A displacement-controlled incremental load was applied over an area of 200×200 mm (8×8 in.) simulating the wheel print impression on the deck slab. The prestressing force was modeled as an external load or pressure whose magnitude equaled the required transverse prestressing level in the deck for a particular analysis. The boundary constraints for the girders were kept the same as in the actual experiments.

Iteration method and convergence criteria

Both physical and geometrical nonlinearities were applied to the system. An incremental-iterative procedure was used for the nonlinear analysis and modified Newton Raphson method was used for the solution. As a first step, the prestressing load was applied followed by displacement-controlled wheel print load (in small steps) with force and energy-based convergence criterion.

Comparison of experimental and numerical results

Ultimate loads

The ultimate punching loads from the experiments (P_T) and finite element analysis (P_{FEA}) are summarized and compared in **Table 3**. The average ratio of P_T/P_{FEA} is 1, the standard deviation is 0.10 and the coefficient of variation is 10%. It can be observed that an increase in the TPL increased the punching shear capacity regardless of what type and position of load was applied. Generally, for single load tests, the finite element approach gave conservative results, while for double loads, the finite element bearing capacities were over-estimated but within reasonable limits as compared to the experimental results. A difference of 21% was observed between the experimental and numerical ultimate loads for test BB12 but this was because of premature failure of that test.

Load – Deflection

The load – deflection behavior of typical cases is shown in **Figure 9**. In general, the initial behavior observed in the load–deflection curves are comparable with the experimental results. After the initial cracking, the load-deflection response in the finite element simulations generally seems to be stiffer than the experimental observations leading to lower deflections. Such over-stiffness could be because of stress-locking in the smeared crack model. Another possible reason can be the fact that the interfaces were not modeled separately for the girder flange-deck slab connection and therefore, the crack at either side of the top of the deck slab panel that was experimentally observed could not be simulated discretely in the finite element analyses. The load – deflection behavior has been discussed in detail in Amir.[5]

Cracking loads and cracking pattern

All the test cases showed a typical punching shear cracking pattern in the finite element analyses and the cracking loads showed good correlation with the experimental observations (see **Figure 10, 11**). The step-by-step development of the cracking pattern in FEA along with comparison of initial cracking loads and inclined shear cracking loads is described in Amir.[5]

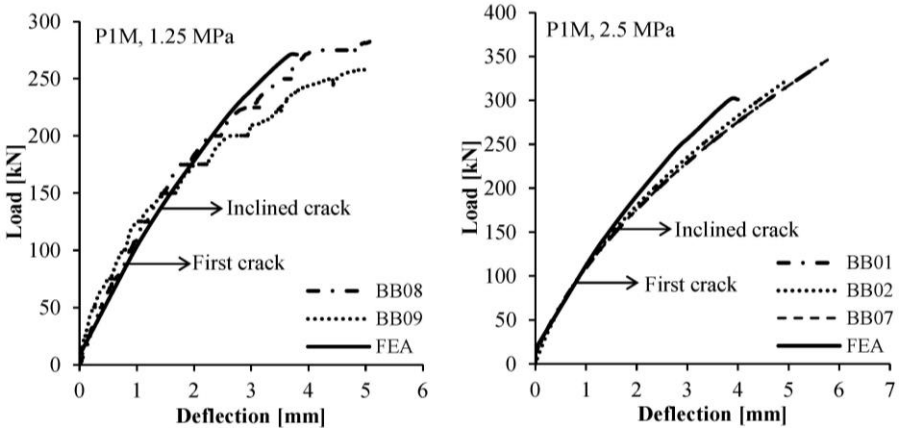

(a)

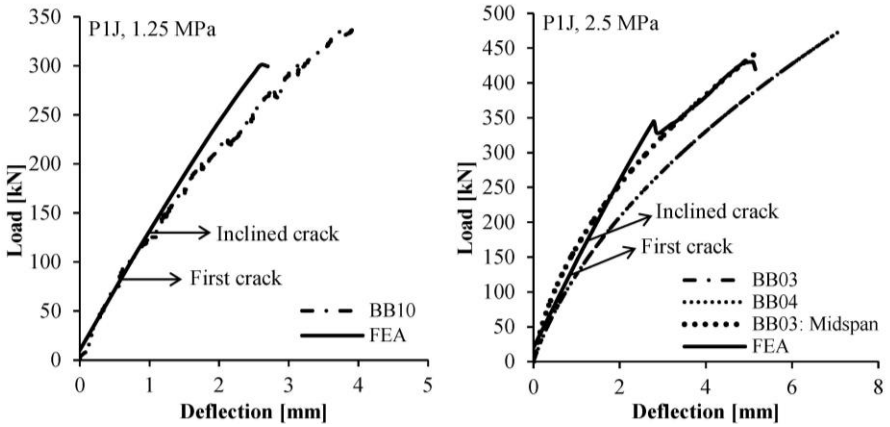

(b)

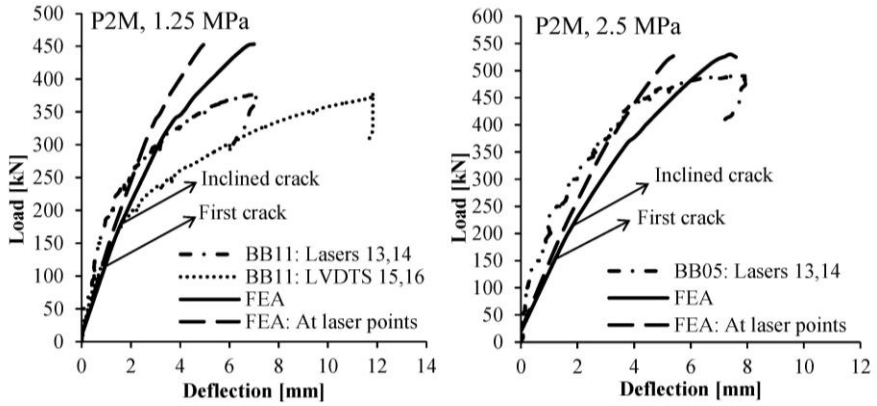

(c)

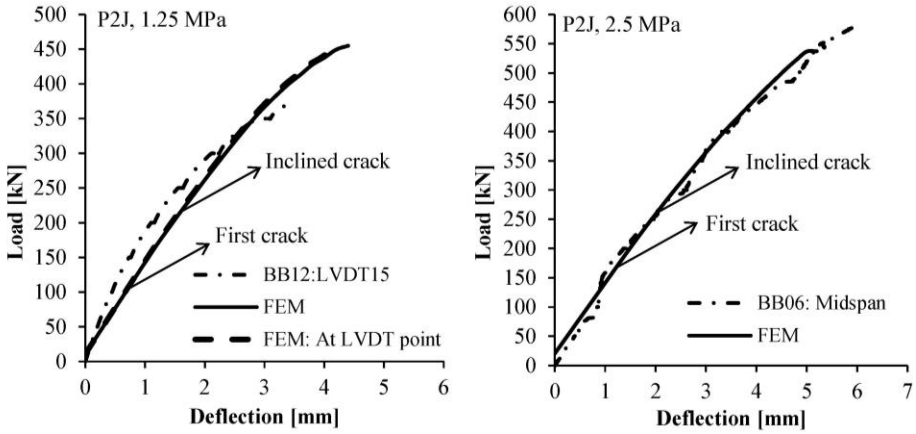

(d)

Figure 9 – Comparison of the load – deflection behavior of typical load cases as observed in experimental and finite element analysis: a) Single wheel print load acting at midspan of deck slab panel, P1M; b) Single wheel print load acting close to the girder flange-slab interface, P1J; c) Double wheel print load acting at midspan of deck slab panel, P2M; d) Double wheel print load acting close to the girder flange-slab interface, P2J. Note: 1 mm = 0.04 in ;1 MPa = 145 psi; 1 kN = 0.225 kip.

Size effect

Bazant and Cao[24] state that the nominal strength decreases with an increase of the structural size. This phenomenon is termed as size effect in literature. A 3D finite element real bridge model (RB4ELEM) was constructed in DIANA to study the size effect on the bearing capacity [**Figure 12(a), 12(b)**].

The main features of the real bridge finite element model are mentioned below:

- The bridge model consisted of four girders, three deck slab panels and two transverse beams. The girders and the transverse beams were analyzed in the linear range while the deck slab was analyzed nonlinearly.
- The girders were 3000 mm (120 in.) high with a web thickness of 200 mm (8 in.). The top flange was 1500 mm (60 in.) and the bottom flange was 580 mm (23 in.) wide.
- Each deck slab was 2100 mm (84 mm) wide and 12 m (40 ft) long with a thickness of 200 mm (8 in).
- 400 mm (16 in.) wide transversely prestressed end transverse beams were modeled close to the supports.
- Four ducts of 50 mm (2 in.) diameter were modeled in central region of the transverse direction in the deck slab at a spacing of 800 mm (32 in.) c/c. This is where the load was also applied.

- The top and bottom horizontal grid consisted of a thickness of 0.25 mm (0.01 in.) and 0.2 mm (0.008 in.) in x and y directions respectively. The vertical grid consisted of a thickness of 0.2 mm (0.008 in.) in the y direction.
- A similar transverse prestressing level was applied to the real bridge deck model (RB4ELEM) as in the scaled bridge deck model (2ELEM). The displacement load applied to the deck was spread over an area of 400×400 mm (16×16 in.), similar to the wheel print area for a real case given for Load Model 1 in EN 1991-2:2002.[10]
- The modeling technique, the mesh size, the element type, the material properties and the nonlinear analysis parameters remained the same as in the 2ELEM model. However, assuming that the real bridge has a larger aggregate size than the model bridge deck, a fracture energy of 0.175 N/mm (1 lb/in) was used in the analyses.

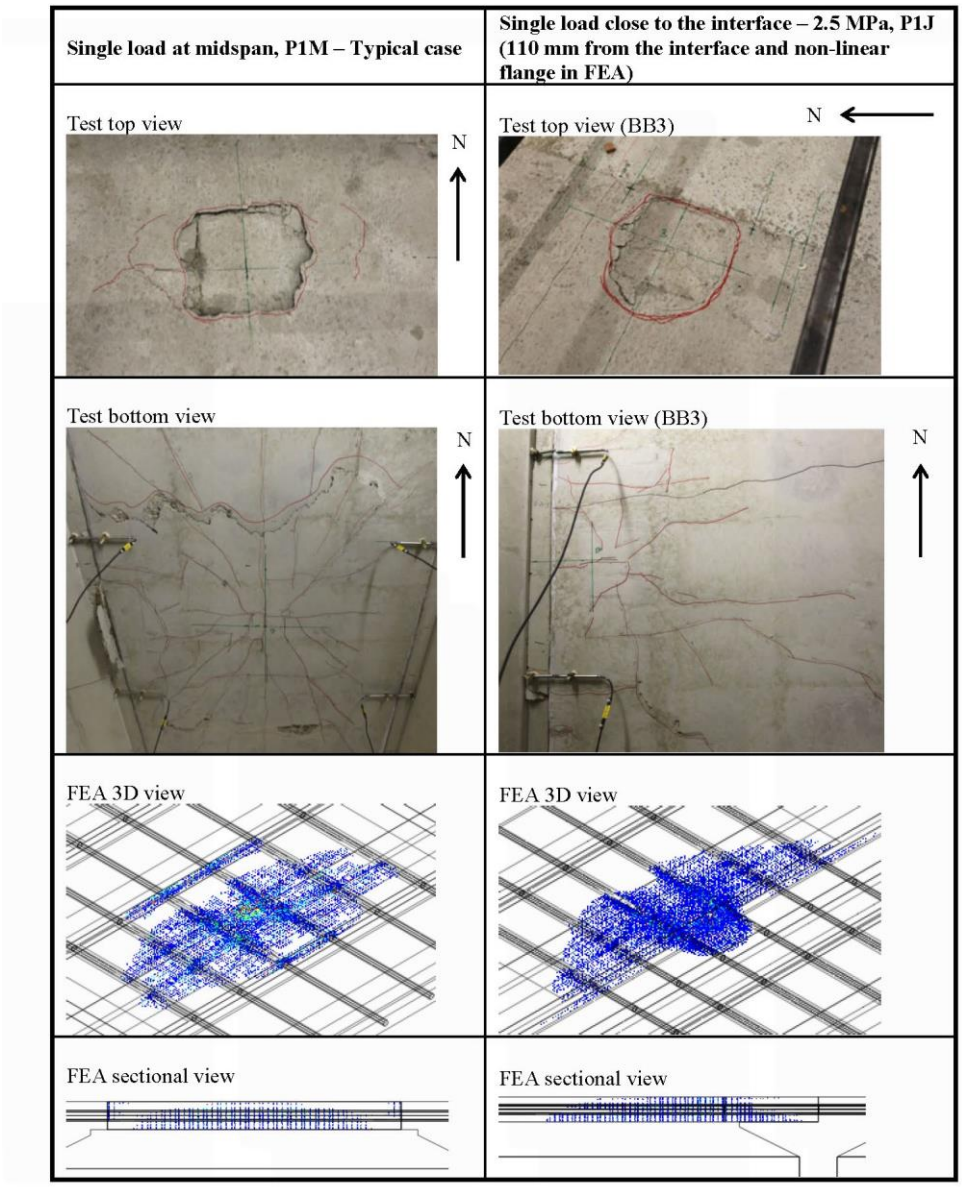

Figure 10 - Comparison of experimental and FE cracking pattern at the failure/ultimate stage for typical single load cases (P1M and P1J).

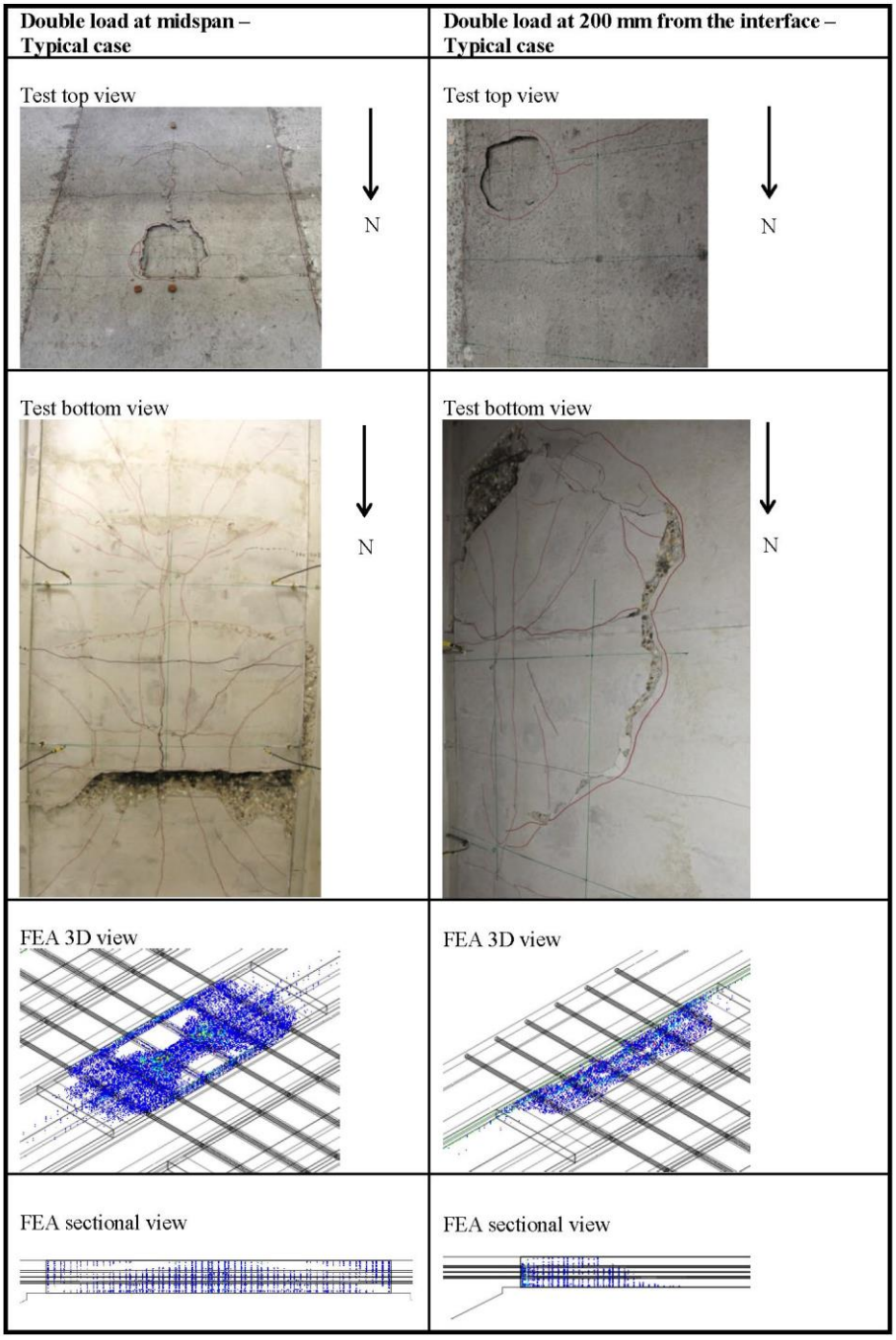

Figure 11 - Comparison of experimental and FE cracking pattern at the failure/ultimate stage for typical single load cases (P2M and P2J).

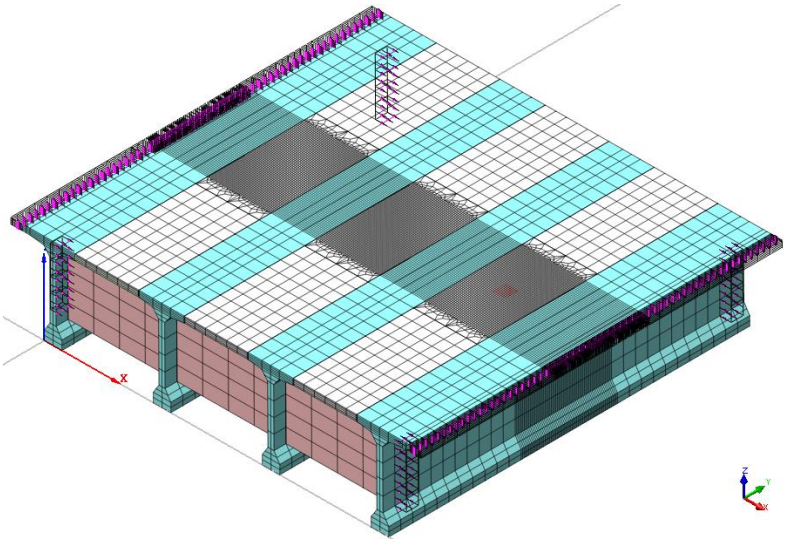

(a)

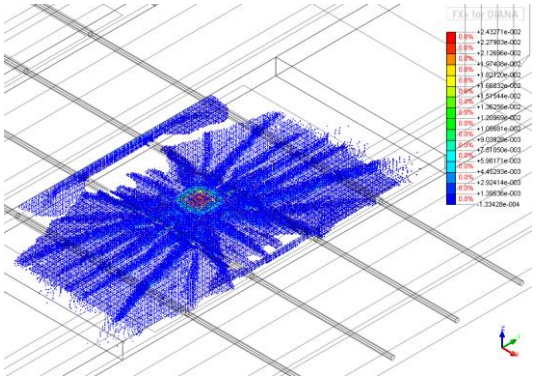

(b)

Figure 12 – The real bridge numerical analyses: a) The 3D solid finite element real bridge model (RB4ELEM); b) Punching shear failure.

Summary of analysis results for the RB4ELEM model

A single load at midspan (P1M) of the exterior panel was applied to the real bridge model with the transverse prestressing levels of 0.5, 1.25 and 2.5 MPa (72.5, 181.25 and 362.5 psi respectively) and was analyzed nonlinearly. All other parameters remained the same. The main results are summarized in the **Table 4**. It can be observed that when a single load acts on the transversely prestressed real bridge deck model (RB4ELEM), punching shear failure occurs [**Figure 12(b)**] and a higher TPL leads to a higher punching shear capacity. The initial flexural cracking load, the initial inclined shear cracking load, and the in-plane force (sum of the transverse prestressing force and the compressive membrane force) are also improved by increasing the TPL.

Calculation of the size factor

For the calculation of the size factor, the ultimate loads of the 2ELEM model and those of RB4ELEM model are compared. Since the RB4ELEM model had 50 mm (2 in.) Φ ducts (size of the ducts in a real bridge), a 2ELEM model with 25 mm (1 in.) Φ ducts is used for the calculation of the size factor. For the sake of comparison, results with 2ELEM *basic* model (used for the numerical analysis of the experimental model bridge) with 45 mm (1.8 in.) Φ ducts are also presented.

Table 4 – Summary of analysis results for the RB4ELEM model

Test RB.	TPL	$P_{FEA,RB}$	$S_{FEA,RB}$	$P_{CR,FEA}$	$P_{CRS,FEA}$	N_{xx}	FMODE
	[MPa]	[kN]	[mm]	[kN]	[kN]	[N/mm]	
1.	0.5	678.3	3.6	240	328.3	486	Brittle punching
2.	1.25	957.5	6.1	277	368.4	864	
3.	2.5	1228.8	7.6	295.3	397	1240	

Note: $P_{FEA,RB}$ = Real bridge FEA ultimate load; $S_{FEA,RB}$ = Real bridge FEA ultimate deflection; $P_{CR,FEA}$ = FEA initial cracking load; $P_{CRS,FEA}$ = FEA Initial inclined shear cracking load; N_{xx} = In-plane force; FMODE = Failure mode; 1 MPa = 145 psi; 1 kN = 0.225 kip; 1 mm = 0.04 in.

Table 5 shows the size factors for a level of 0.5, 1.25 and 2.5 MPa (72.5, 181.25 and 362.5 psi respectively) transverse prestressing considering the 2ELEM model with 25 mm (1 in.) and 45 mm (1.8 in.) Φ ducts. It is interesting to note that the size factor seems to be dependent on the level of transverse prestressing and reduces for a higher TPL. Regan[25] states that if the same concrete mix is used in the specimens of varying depth while the maximum aggregate size is scaled along with the depth, the size effect is somewhat reduced. In the current study, the same concrete strength but different fracture energies were used for the scaled 2ELEM and real bridge RB4ELEM models (considering a larger aggregate size for the RB4ELEM model than the 2ELEM model), therefore some effect of the size has already been considered. Smaller size factors are obtained when the projected capacity of 45 mm (1.8 in.) Φ ducts 2ELEM model is compared with the real bridge capacity.

Table 5 – The size factor calculated from numerical results

TPL	$P_{pr,FEA}$		$P_{FEA,RB}$	Size factor normalized for 200 mm thick slab	
	25 mm ducts	45 mm ducts	50 mm ducts	25 mm ducts	45 mm ducts
[MPa]	[kN]	[kN]	[kN]	$P_{pr,FEA}/P_{FEA,RB}$	$P_{pr,FEA}/P_{FEA,RB}$
0.5	1104	1016	678.3	1.63	1.5
1.25	1168	1086	957.5	1.22	1.13
2.5	1332	1209	1228.8	1.08	0.98

Note: $P_{pr,FEA}$ = finite element model bridge (2ELEM) projected ultimate load by force scale factor $x^2 = 2^2$, $P_{FEA,RB}$ = Real bridge FEA ultimate load; 1 MPa = 145 psi; 1 kN = 0.225 kip; 1 mm = 0.04 in.

THEORETICAL ANALYSIS

Punching shear capacity without CMA for the model bridge deck

The punching shear capacity of single load tests with failure in brittle punching is calculated according to the background report 25.5-02-37-prENV 1992-1-1[26] and ACI 318-19[27]. The TPLs investigated are 0.5, 1.25 and 2.5 MPa (72.5, 181.25, 362.5 psi). The mean material properties used are described in **Table 1**. No material factors have been used.

The background report 25.5-02-37-prENV 1992-1-1[26] calculates the design punching shear capacity as:

$$v_{Rd,c} = C_{Rd,c} k (100 \rho_l f_{ck})^{1/3} + k_1 \sigma_{cp} \left[SI\ Units: N, mm \right] \quad (1)$$

$$V_{r,EC2} = v_{rd,c} u d \left[SI\ Units: N, mm \right] \quad (2)$$

where, $C_{Rd,c} = 0.18 / \gamma_c$, ($\gamma_c = 1$ as no material factors are used), $k = 1 + (200/d)^{1/2} \leq 2$ is the size factor, $\rho_l = (\rho_{ly}\, \rho_{lz})^{1/2} \leq 0.02$ is the longitudinal reinforcement ratio, f_{ck} is the characteristic concrete cylinder strength, $k_1 = 0.08$[26], $\sigma_{cp} = (\sigma_{cy} + \sigma_{cz})/2$ is the normal compressive stress in concrete, $V_{r,EC2}$ is the punching shear load, $u = 4c + 4\pi d$ is the critical shear perimeter calculated at $2d$ from the face of the square column or the loaded area with side length c and d = average effective depth in each orthogonal direction. Furthermore, σ_{cy} and σ_{cz} are the normal concrete stresses from longitudinal forces in the critical section in the y and z-directions respectively and ρ_{ly} and ρ_{lz} relate to the bonded steel in the y and z-directions respectively.

The ACI 318-19[27] punching shear equation is:

$$V_{c,ACI} = (0.29\sqrt{f_{cm}} + 0.3\sigma_{cp}) b_0 d \left[SI\ Units: N, mm \right] \quad (3)$$

where, 0.9 MPa ≤ σ_{cp} ≤ 3.5 MPa (130.5 psi ≤ σ_{cp} ≤ 507.5 psi) is the average prestressing in each direction, the mean concrete cylinder strength f_{cm} < 35 MPa (5075 psi). b_0 = 4 (c + d) is the length of the control perimeter at d/2 from the face of the column or the loaded area with side length c, and d is the effective depth. The limitation on σ_{cp} has been ignored here. Calculations are done for both f_{cm} = 35 MPa (5075 psi) and 65 MPa (9425 psi).

Figure 13 shows that the basic equations used for both codes underestimate the punching shear capacity of laterally restrained prestressed slabs. This is attributed to the ignorance of CMA that is present in such slabs. However, it can be observed that the capacity prediction for ACI 318, $V_{r,ACI}$ (65 MPa), when the limit on f_{cm} is not followed is better, although still conservative for higher TPLs. For 0.5 MPa (72.5 psi), it is comparable with the test results. Meanwhile, the results from background report 25.5-02-37-prENV 1992-1-1 ($V_{r,EC2}$) are conservative even for a very low level of 0.5 MPa (72.5 psi) TPL. It is obvious that the contribution of prestressing (σ_{cp}) is low in both ACI 318 and the background report Eurocode 2.

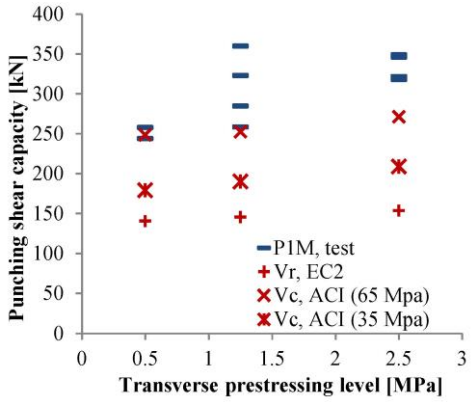

Figure 13 – Comparison of experimental punching shear capacity for a single load at midspan of deck slab panel (P1M, test) with that of background report 25.5-02-37-prENV 1992-1-:2002 ($V_{r,EC2}$) and ACI 318 ($V_{r,ACI}$). Note: 1 kN = 0.225 kip; 1 MPa = 145 psi.

Punching shear capacity without CMA for the real bridge

Calculations using existing methods and codes are also made for a full-scale bridge deck whose structural details are given in previous section. The background report 25.5-02-37-prENV-1992-1-1:2002[26] and ACI 318-19[27] are used to assess the capacity without considering CMA. **Table 6** shows the punching shear capacity for the real bridge using the aforementioned codes. Mean material strengths are used with no material factors. Comparison is also made with the finite element analyses results presented in the previous section.

Table 6 – Calculated punching shear capacity of the real bridge using various codes and finite element analyses

#	TPL	$V_{r,EC2}$		$V_{c,ACI}$		$P_{FEA,RB}$
	[MPa]	[kN]	[kN]	[kN]	[kN]	
		$k \leq 2$	$k > 2$	f_{cm} = 35 MPa	f_{cm} = 65 MPa	
1	0.5	484	510	652*	879*	678
2	1.25	502	528	693	920	957.5
3	2.5	531	557	761	988	1229

Note: $V_{r,EC2}$ = Punching capacity from the background report Eurocode 2; $V_{c,ACI}$ = Punching capacity from ACI 318; $P_{FEA,RB}$ = Real bridge FEA ultimate load (punching capacity); *σ_{cp} < 0.9MPa. The limit on the minimum prestress has been ignored in these calculations; 1 MPa = 145 psi; 1 kN = 0.225 kip.

The background report 25.5-02-37-prENV 1992-1-1 (2002)

It can be observed in **Table 6** that the background report Eurocode 2 gives the lowest capacity out of all the methods. With an increasing transverse prestressing level, the difference with the finite element results grows.

Calculations have been made by first keeping the limit on the size factor ($k \leq 2$) in the first column and then ignoring the limit ($k > 2$) in the second column. Slightly higher capacities are achieved when the limit on the size factor is ignored.

ACI 318 (2019)

The ACI 318 has limitations on σ_{cp} and f_{cm} and does not consider a size effect. In the first column the limitation on f_{cm} is followed and in the second it is ignored. The first column results are on the conservative side except for 0.5 MPa (72.5 psi) which compares well with the FEA result although for higher TPLs, the results are underestimated again. The second column results seem reasonable for 1.25 MPa (181.25 psi) but at the conservative side for 2.5 MPa (362.5 psi). The increase in capacity that is seen in the second column is the result of ignoring the limit on f_{cm} rather than increasing the prestressing contribution. As a result, the punching shear capacity for 0.5 MPa (72.5 psi) is grossly overestimated. It is clear that the current codes are not fully suitable for the prediction of the punching shear capacity of prestressed slabs considering compressive membrane action and there is a dire need to develop a method for such cases.

Model Code 2010 punching shear provisions: The Critical Shear Crack Theory (CSCT)

In this section an attempt will be made to apply the Critical Shear Crack Theory (CSCT)[28,29] on the transversely prestressed bridge deck under study using the Levels of Approximation[30,31] approach with some modifications. The punching shear provisions for prestressed slabs from the Model Code 2010[9] using CSCT will be used in combination with numerically found in-plane forces comprising compressive membrane action.

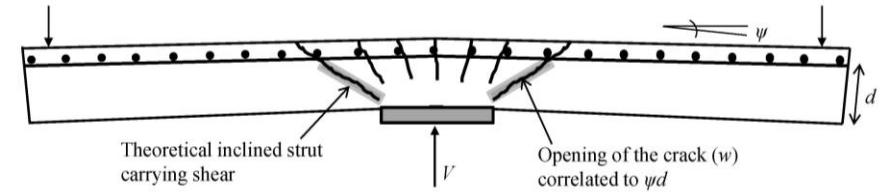

(a)

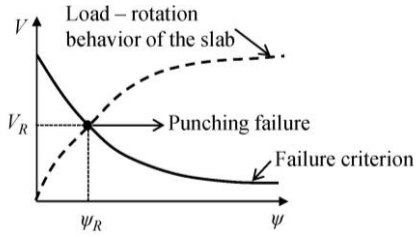

(b)

Figure 14 – The Critical Shear Crack Theory (CSCT)[28]: a) The basic mechanism; b) Calculation of strength and deformation capacity.

Failure criterion

According to the CSCT, the width of the critical shear crack can be correlated to the product of the rotation and the flexural effective depth of the slab ($w \propto \psi d$), [**Figure 14(a), 14 (b)]**. **Eq. 4** gives the failure criterion of the Critical Shear Crack Theory. This equation does not involve any material factors and is based on mean strengths.

$$\frac{V_R}{b_0 d_v \sqrt{f_{cm}}} = \frac{3/4}{1+15\dfrac{\psi d}{d_{g0}+d_g}} \left[SI\ Units: N, mm\right] \quad (4)$$

where V_R is the shear strength, b_0 is the length of the control perimeter at $d_v/2$ of the edge of the supported area, d_v is the shear-resisting effective depth of the member, f_{cm} is the mean compressive strength of the concrete, ψ is the rotation and is calculated depending on the required level of approximation (LoA), d is the flexural effective depth of the member, d_{g0} is the maximum aggregate size and d_g is the reference aggregate size equal to 16 mm (0.64 in.). For the calculations, mean values of material strengths will be used with no material factors. For openings and inserts, the basic control perimeter b_0 is recommended to be reduced[9] but the presence of ducts in the current problem has been ignored while calculating b_0. The possibility of flexural failure has been ruled out of the iterative procedure, since no such failure was observed in the tests or the FEA. For the model bridge deck calculations, tests done above the ducts and the control tests with 0.5 MPa (72.5 psi) TPL have not been considered.

Load-rotation relationship of the prestressed slab

The rotation at failure (ψ in **Eq. 4**) can be evaluated by using the Levels-of-Approximation (LoA) approach. Higher the level of approximation, more precise the calculation. In the Model Code 2010, the influence of prestressing (**Figure 15**) on punching shear strength is explored at the LoA II and III (typical LoA to be used for structures where punching shear strength is governing). No calculations are made at LoA I for prestressed slabs. In LoA IV, the rotation ψ can be calculated on the basis of a nonlinear flexural analysis of the structure and accounting for cracking, tension-stiffening effects, yielding of the reinforcement and any other non-linear effect relevant for providing an accurate assessment of the structural bearing capacity[9].

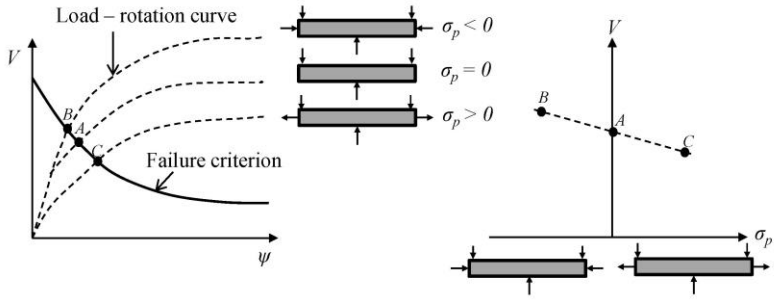

Figure 15 – The Critical Shear Crack Theory: Influence of an in-plane force σ_p on the punching shear capacity V[29]. Note: 1 kN = 0.225 kip; 1 MPa = 145 psi.

Ultimate bearing capacity of the model bridge deck by CSCT with modified LoA approach

For the assessment of the ultimate bearing (punching shear) capacity of the model bridge deck, an iterative procedure needs to be carried out to find the intersection point of the failure criterion and the load-rotation curve of the slab representing the available punching shear strength and the shear force for a given rotation, respectively. Instead of using the traditional LoA approach[30,31], a different criterion will be introduced to calculate the capacity of the model bridge deck. The following general equation will be used to calculate the rotations.

$$\psi = 1.5\frac{r_s}{d}\frac{f_{sy}}{E_s}\left(\frac{m_s - m_P}{m_R - m_P}\right)^{1.5} \qquad (5)$$

In **Eq. 5**, $m_s \approx V/8$, for inner columns without unbalanced moments[28,29], $m_R = \rho f_{sy} d^2 (1 - 0.5\rho f_{sy}/f_{cm})$ and $m_P = n (h/2 - d/3 + e)$. Here, V is the acting shear force, ρ is the steel reinforcement ratio, f_{sy} is the yield strength of the steel, f_{cm} is the mean compressive cylinder strength of concrete, n is the normal force per unit length, h is the depth of the slab, d is the effective depth and e is the eccentricity of the normal force from the center of gravity of the section. As a sign convention, the decompression moment is considered positive when it leads to compressive stresses on the top side of the slab[29]. For the current case, no eccentricity exists since the prestressing bars are applied at mid-depth. ρ_{ps} (geometric prestressing steel ratio) and f_{pe} (effective prestress) representing an equivalent steel will be used in place of ρ and f_{sy}, respectively, to determine the flexural strength of the deck slab panel with unbonded transversely prestressed bars. The flexural effective depth of the model bridge deck will be taken equal to the shear resisting effective depth in the assessment calculations ($d = d_v$ = 87 mm (3.48 in.)).

Elementary Level of Approximation
The load-rotation relationship is established using the transverse prestressing force as the normal force *n*. This serves as a lower bound for the ultimate capacity (**Figure 16**).

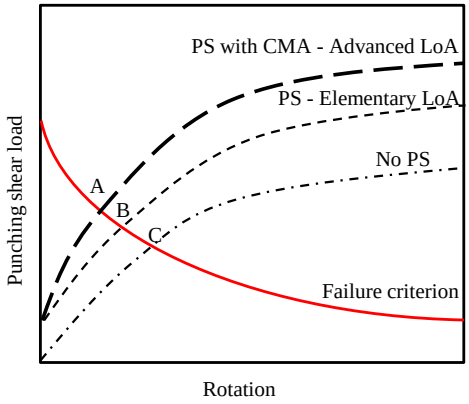

Figure 16 – The Level of Approximation approach (LoA) for the analysis of the transversely prestressed deck slab (PS = Prestressing, CMA = Compressive membrane action). The elementary LoA giving punching shear load B and the advanced LoA giving punching shear load A. For no prestressing, the failure load is C.

Advanced Level of Approximation
The load-rotation relationship is established using the overall in-plane force (sum of transverse prestressing force and compressive membrane force) as the normal force *n*, found from the nonlinear analyses of the 3D solid, finite element model bridge (N_{xx} from composed elements). This serves as the upper bound of the ultimate capacity and compressive membrane action is automatically incorporated in the load-rotation relationship (**Figure 16**).

Comparison of the theoretical, experimental and FEA punching loads
A comparison is drawn between the punching shear capacity obtained theoretically from the critical shear crack model and the results of the experimental and finite element analysis, see **Table 7**. A coefficient of variation of 11% and 9% is obtained when the experimental and the FEA punching loads are compared with the advanced LoA results, respectively.

Size factor and ultimate bearing capacity of the real bridge by CSCT with modified LoA approach
The ultimate capacity of the real, full scale bridge can be estimated by the CSCT in a similar way as for the scaled model bridge. In order to calculate the size effect, the results of CSCT regarding the model bridge (from **Table 7**) are projected using the force scale factor $(x^2=2^2)^5$ to obtain the real bridge capacity as shown in **Table 8.** The size factors calculated from the FEA model bridge results are also given.

It can be observed from **Table 8** that when comparing the projected CSCT model bridge results with the actual calculated CSCT capacity of the real bridge, the size factor is approximately equal to 1 (in sharp contrast to FEA results where a size effect is observed). **Eq. 4** shows that the size effect has been introduced in the CSCT by multiplying the slab rotation ψ by its thickness d which cancels out when the ψ of the **Eq. 5** is put into **Eq. 4**. Muttoni[28] concludes that the reduction of the strength for size effect is not a function of the slab thickness but rather of the span, represented by the radius r_s defined as the distance from the axis of the column to the line of contra-flexure of the bending moments. Therefore, for further calculations based on CSCT, no size factor is required. However, for calculations based on FEA, considering that the maximum average size factor obtained from the FEA is 1.15, a factor of 1.2 is selected conservatively and is also used for the model bridge experimental results. It should be noted that Mitchel et al.[32] show a size factor of 1.2 for an effective depth of 100 mm (4 in.) when the shape of the size effect expressions from various design codes are normalized to give a size factor of 1 for an average effective depth of 200 mm (8 in.).

Table 7 – Comparison of the CSCT punching loads with the experimental and FEA results for the model bridge

Test BB.	TPL	Designation	P_T	P_{FEA}	P_{CSE}	P_{CSA}	P_T/P_{FEA}	P_T/P_{CSA}	P_{FEA}/P_{CSA}
	[MPa]		[kN]	[kN]	[kN]	[kN]			
1.	2.5	C-P1M	348.7	302.3	253	311	1.15	1.12	0.97
2.	2.5	A-P1M	321.4	302.3	253	311	1.06	1.03	0.97
3.	2.5	A-P1J	441.6	429.9	253	422.4	1.03	1.05	1.02
4.	2.5	C-P1J	472.3	429.9	253	422.4	1.10	1.12	1.02
5.	2.5	C-P2M	490.4	529.9	362.2	453.3	0.93	1.08	1.17
6.	2.5	A-P2J	576.8	537.0	362.2	482.3	1.07	1.20	1.11
7.	2.5	C-P1M	345.9	302.3	253	311	1.14	1.11	0.97
8.	1.25	C-P1M	284.5	271.4	220.2	295.7	1.05	0.96	0.92
9	1.25	A-P1M	258.2	271.4	220.2	295.7	0.95	0.87	0.92
10.	1.25	A-P1J	340.3	300.7	220.2	310.9	1.13	1.09	0.97
11.	1.25	C-P2M	377.9	453.4	314.7	431.3	0.83	0.88	1.05
12.	1.25	A-P2J	373.7	454.9	314.7	432.1	0.82	0.86	1.05
16.	2.5	B-P2M	553.4	592.7	362.2	482.3	0.93	1.15	1.23
19.	2.5	B-P1M	317.8	306.0	220.9	281.9	1.04	1.13	1.09
			Mean				**1.02**	**1.05**	**1.03**
			Standard deviation				**0.11**	**0.11**	**0.09**
			Coefficient of variation				**0.11**	**0.11**	**0.09**

Note: P_T = Test failure load; P_{FEA} = Finite element ultimate load; P_{CSE} = CSCT elementary LoA ultimate punching load; P_{CSA} = CSCT advanced LoA ultimate punching load; 1 MPa = 145 psi; 1 kN = 0.225 kip.

Table 8 – The size factor calculated from CSCT and modified LoA approach

TPL	$P_{pr,CSE}$	$P_{pr,CSA}$	$P_{CSE,RB}$	$P_{CSA,RB}$	Size factor FEA		Size factor CSCT	
	Scale factor $x = 2^2$	Scale factor $x = 2^2$			25mm ducts	45mm ducts	$P_{pr,CSE}/P_{CSE,RB}$	$P_{pr,CSA}/P_{CSA,RB}$
[MPa]	[kN]	[kN]	[kN]	[kN]				
1.25	881	1183	891.5	1141	1.22	1.13	0.99	1.04
2.5	1012	1244	1018	1240	1.08	0.98	0.99	1.00
			Average		**1.15**	**1.1**	**≈ 1**	**≈ 1**

Note: $P_{pr,CSE}$ = Projected CSCT elementary LoA ultimate punching load for the real bridge; $P_{pr,CSA}$ = Projected CSCT advanced LoA ultimate punching load for the real bridge; $P_{CSE,RB}$ = Real bridge CSCT elementary LoA ultimate punching load; $P_{CSA,RB}$ = Real bridge CSCT advanced LoA ultimate punching load; 1 MPa = 145 psi; 1 kN = 0.225 kip.

Safety Analysis of the Real bridge

One of the main objectives of this research study is to perform the safety analysis of the real (full scale) bridge. While the numerical results of the analyses carried out on the real bridge can be used directly to evaluate the capacity (**Table 6**) after applying the necessary safety factors, the experimental results, based on the 1:2 scaled model of the real bridge, still need to be projected to obtain the capacity of the full-scale bridge.

In this section, the numerical and experimental results will be projected using all safety factors and compared with the design wheel loads to assess if the real structure is able to carry the modern traffic loads. Both the numerical analyses results of the 1:2 scaled model (2ELEM) and the real bridge model (RBELEM) will be used. In order to keep similarity between the experimental and numerical results, the 2ELEM model with 45 mm (1.8 in.) ducts will be used here. This will be a lower bound of the capacity obtained via the numerical analyses. Realistically, the 2ELEM 25 mm (1 in.) Φ ducts model is the 1:2 scaled model for RBELEM 50 mm (2 in.) Φ ducts model. Also results with 0.5 MPa (72.5 psi) have not been considered since they were performed only as control cases and such a low level of TPL does not exist in the type of the bridge under study. Analyses with wheel print above the ducts have also been disregarded although they give a higher capacity.

The Global Safety format and model uncertainty

Generally, the global resistance factor (GRF) is considered the most promising format to be used for concrete structures since it is easy to use with an adequate safety margin.[33] The nonlinear analysis is performed using mean values for the material characteristics and geometrical properties. The ultimate limit state verification requires a comparison of design resistance and design loads expected on the structure. The design equation is:

$$F_d < R_d \tag{6}$$

where, F_d is the design action and R_d is the design resistance. Both the action and resistance have individual safety margins incorporated into them[33]. The safety margin for the resistance part can be expressed as:

$$R_d = \frac{R_m}{\gamma_{GL}} \tag{7}$$

The calculated resistance R_m, using mean values for the material strengths, is divided by a global resistance factor, γ_{GL}, to obtain the design value for the structural resistance R_d. The guidelines for the nonlinear finite element analysis of concrete structures (RTD 1016)[22] give $\gamma_{GL} = 1.2 \times 1.06 = 1.27$, where γ_{GL} is the product of the safety and the model coefficients. However, the mean resistance in the Model Code 2010[9] and in RTD 1016[22] is based on fictitious values ($f_{cm} \approx 0.85\ f_{ck}$) and not the actual mean strengths. In the present study, since the actual mean strengths are used, therefore, γ_{GL} is further divided by 0.85 to obtain a factor of 1.5 ($\gamma_{GL'} = 1.27/0.85 = 1.5$). The design load F_d is obtained by multiplying the characteristic load with a partial factor γ_Q. The characteristic wheel load, Q_K according to the Load Model 1of EC2[3] is 150 kN (33.75 kips) for a single wheel (300 kN (67.5 kips) for a double load) and 300 kN (67.5 kips) for an axle. Hence the actions part of Eq. 6 can be rewritten as:

$$F_d = \gamma_Q Q_K \tag{8}$$

The Ministry of Infrastructure and the Environment in the Netherlands, Rijkswaterstaat, allows a partial factor for traffic actions γ_Q of 1.25 for existing bridges built before 2012 in RBK Table 2.1 from RTD 1006:2013[34] but a partial factor of 1.5 according to EN 1990+A1+A1/C2:2011/NB:2011 (Table NB.13-A2.4(B), CC3)[35] for new bridges is used here conservatively.

Factor of safety

In this section, the factor of safety of the model bridge and the real bridge against the design wheel load of the Eurocode 2 will be evaluated as per **Eq. 6, Eq. 7** and **Eq. 8**.

Using the 1:2 scaled model bridge deck analyses results

There are two approaches by which factor of safety can be calculated from the results of 1:2 scaled model bridge deck analyses. The first approach[36] is to use the actual results as the resistance of the model bridge deck, calculate the design resistance and compare it with the *scaled down* Eurocode design wheel load. The factor of safety thus obtained is applicable for the model bridge deck. The second approach (which is explained in this paper) is to *scale up* (or to project) the actual results by using the scale and size factors to get the resistance of the real bridge, calculate the design resistance and compare it with the Eurocode design wheel load. The factor of safety thus obtained is applicable for the real bridge.

Using actual analyses results to calculate factor of safety for the model bridge deck: The resistance R_m is taken equal to the ultimate (punching) loads from the tests, the finite element results and the critical shear crack theory results at an advanced LoA (P_T, P_{FEA} and P_{CSA} respectively) from the analyses of the 1:2 scaled bridge model. The test design resistance $R_{md,T}$ is calculated by applying Level II method[4] on the test ultimate load P_T ($\gamma_T = \mu_{RD}/B_{RD} =$

[3] The ultimate distributed load is not taken into account. Also, the Load Model 2 of Eurocode 2 is not being considered, as the wheel footprint of only Load Model 1 was used in all the analyses.

[4] $B_{RD} = \mu_{RD}(1-\alpha_{BR}\beta\delta_{BR})$, where $\alpha_{BR} = 0.8$, $\beta = 3.8$ and $\delta_{BR} = 0.11$, see Table 8.6. Therefore, $\gamma_T = \mu_{RD} / B_{RD} = 1.5$.

1.5). The FEA design resistance $R_{md,FEA}$ is obtained by dividing P_{FEA} by $\gamma_{GL'}$ (1.5). Design resistance using CSCT[5] $R_{md,CSA}$ is calculated for the model bridge deck at an advanced LoA with the appropriate material and safety factors. The scaled down design wheel load F_{md} is obtained by multiplying the characteristic load Q_K with a partial factor γ_Q (1.5) and dividing by the force scale factor ($x^2 = 2^2$). The factor of safety (FOS) is obtained by dividing the design loads with the design resistance (see **Table 9**).

Table 9 – Calculation of the factor of safety for the model bridge deck using the actual analyses results

BB	TPL	P_T	P_{FEA}	P_{CSA}	$R_{md,T}$	$R_{md,FEA}$	$R_{md,CSA}$	Test FOS	FEA FOS	CSCT FOS
					P_T/γ_T	$P_{FEA}/\gamma_{GL'}$		$R_{md,T}/F_{md}$	$R_{md,FEA}/F_{md}$	$R_{md,CSA}/F_{md}$
	[MPa]	[kN]	[kN]	[kN]	[kN]	[kN]	[kN]			
1.	2.5	348.7	302.3	311	232	202	236	4.13	3.58	4.20
2.	2.5	321.4	302.3	311	214	202	236	3.81	3.58	4.20
3.	2.5	441.6	429.9	422.4	294	287	328	5.23	5.10	5.83
4.	2.5	472.3	429.9	422.4	315	287	328	5.60	5.10	5.83
5.	2.5	490.4	529.9	453.3	327	353	351	2.91	3.14	3.12
6.	2.5	576.8	537.0	482.3	385	358	351	3.42	3.18	3.12
7.	2.5	345.9	302.3	311	231	202	236	4.10	3.58	4.20
8.	1.25	284.5	271.4	295.7	190	181	224	3.37	3.22	3.98
9	1.25	258.2	271.4	295.7	172	181	224	3.06	3.22	3.98
10.	1.25	340.3	300.7	310.9	227	200	236	4.03	3.56	4.19
11.	1.25	377.9	453.4	431.3	252	302	333	2.24	2.69	2.96
12.	1.25	373.7	454.9	432.1	249	303	333	2.21	2.70	2.96
16.	2.5	553.4	592.7	482.3	369	395	376	3.28	3.51	3.34
19.	2.5	317.8	306.0	281.9	212	204	210	3.77	3.63	3.73
			Average Factor of Safety (FOS)					3.65	3.56	3.97

Note: P_T = Test failure load; P_{FEA} = Finite Element Analysis failure load; P_{CSA} = CSCT advanced LoA ultimate punching load; $R_{md,T}$ = Model bridge test design resistance; $R_{md,FEA}$ = Model bridge FEA design resistance; $R_{md,CSA}$ = Model bridge CSCT design resistance; F_{md} = Scaled down design wheel load; 1 MPa = 145 psi; 1 kN = 0.225 kip.

Using projected (scaled up) model bridge deck results to calculate factor of safety for the real bridge deck: The resistance R_m is taken equal to the projected ultimate (punching) loads from the tests and the finite element results ($P_{pr,T}$ and $P_{pr,FEA}$, respectively) that are derived from the experimental and the FEA results of the 1:2 scaled bridge model using the scale and size factors, as shown in **Table 10**. The test design resistance $R_{d,T}$ is calculated by applying Level II method on the projected test results, $P_{Pr,T}$ ($\gamma_T = \mu_{RD} / B_{RD} = 1.5$). The FEA design resistance $R_{d,FEA}$ is obtained by dividing $P_{pr,FEA}$ by $\gamma_{GL'}$ (1.5). Design strength using CSCT calculated for the model bridge deck at an advanced LoA ($R_{md,CSA}$ in **Table 9**) is projected to give design strength of the real bridge, $R_{d,CSA}$ using the scale and size factors. The factor of safety (FOS) is obtained by dividing the design loads with the design resistance.

Using the real bridge deck analyses results

A similar calculation is made for the real bridge (using actual dimensions) from the FEA and the CSCT. $P_{CSA,RB}$ and $P_{FEA,RB}$ will be taken as R_m, the resistance obtained from the CSCT (advanced LoA) and the FEA, respectively. Since these are *direct* analyses results and no projection from the model bridge involving scale factors is made, therefore, no size factor is employed.

The FEA design resistance $R_{d,FEA}$ is obtained by dividing $P_{FEA,RB}$ by γ_{GL} (1.27). $P_{CSA,RB}$ is recalculated using **Eq. 4** and **Eq. 5** (but by using design parameters and involving characteristic strengths and material factors) to obtain CSCT design resistance $R_{d,CSA}$ at the advanced LoA approach (with compressive membrane action). The design load/action, F_d remains the same as defined in **Eq. 8**. The results are shown in **Table 11**.

[5] Refer to the modified LoA approach described in the previous section or in Amir[5].

Table 10 – Calculation of the factor of safety for the real bridge using the projected model bridge analyses

BB.	TPL	$P_{pr,T}$	$P_{pr,FEA}$	$R_{d,T}$	Projected $R_{d,FEA}$	Projected $R_{d,CSA}$	Test FOS	FEA FOS	CSCT FOS
		$P_T \times 2^2/1.2$	$P_{FEA} \times 2^2/1.2$	$P_{pr,T}/\gamma_T$	$P_{pr,FEA}/\gamma_{GL'}$	$R_{md,CSA} \times 2^2/1.2$	$R_{d,T}/F_d$	$R_{d,FEA}/F_d$	$R_{d,CSA}/F_d$
	[MPa]	[kN]	[kN]	[kN]	[kN]	[kN]			
1.	2.5	1162	1008	775	672.0	788	3.44	2.99	3.50
2.	2.5	1071	1008	714	672.0	788	3.17	2.99	3.50
3.	2.5	1472	1433	981	955.3	1093	4.36	4.25	4.86
4.	2.5	1574	1433	1050	955.3	1093	4.66	4.25	4.86
5.	2.5	1635	1766	1090	1177.3	1170	2.42	2.62	2.60
6.	2.5	1923	1790	1282	1193.3	1171	2.85	2.65	2.60
7.	2.5	1153	1008	769	672.0	788	3.42	2.99	3.50
8.	1.25	948	905	632	603.3	746	2.81	2.68	3.32
9	1.25	861	905	574	603.3	746	2.55	2.68	3.32
10.	1.25	1134	1002	756	668.0	786	3.36	2.97	3.49
11.	1.25	1260	1511	840	1007.3	1110	1.87	2.24	2.47
12.	1.25	1246	1516	830	1010.7	1111	1.85	2.25	2.47
16.	2.5	1845	1976	1230	1317.3	1252	2.73	2.93	2.78
19.	2.5	1059	1020	706	680.0	699	3.14	3.02	3.11
			Average Factor of Safety (FOS)				**3.05**	**2.96**	**3.31**

Note: $P_{pr,T}$ = Projected test ultimate punching load ; $P_{pr,FEA}$ = Project FE ultimate punching load; $R_{d,T}$: Real bridge test design resistance; $R_{d,FEA}$ = Real bridge FEA design resistance; $R_{d,CSA}$: Real bridge CSCT design resistance ($R_{md,CSA}$ is taken from Table 9); 1 MPa = 145 psi; 1 kN = 0.225 kip.

Table 11– Comparison of the ultimate capacity and the applied loads of the real bridge using real dimensions

#	TPL	Designation	$P_{CSA,RB}$	$P_{FEA,RB}$	$R_{d,CSA}$	$R_{d,FEA}$	CSCT FOS	FEA FOS
							$R_{d,CSA}/F_d$	$R_{d,FEA}/F_d$
	[MPa]		[kN]	[kN]	[kN]	[kN]		
1.	1.25	P1M	1141	957.5	855.7	753.9	3.8	3.35
2.	2.5	P1M	1240	1228.8	935.7	967.6	4.16	4.30
			Average Factor of Safety (FOS)				**3.98**	**3.83**

Note: $P_{CSA,RB}$ = Real bridge CSCT advanced LoA ultimate punching load; $P_{FEA,RB}$ = Real bridge FEA ultimate punching load; $R_{d,FEA}$ = Real bridge FEA design resistance; $R_{d,CSA}$: Real bridge CSCT design resistance; 1 MPa = 145 psi; 1 kN = 0.225 kip.

Discussion

For the model bridge deck, a factor of safety of 3.65, 3.56 and 3.97 is obtained by using the actual results of experiments, the FEA and the CSCT. For the real bridge deck, a factor of safety (FOS) of 3.05, 2.96 and 3.31 is obtained from the projected results of experiments, the finite element analysis and the CSCT, respectively. By using the real bridge analyses results, a factor of safety (FOS) of 3.98 and 3.83 is obtained from the CSCT and the finite element analyses of the real bridge, respectively. It is remarkable how the FOS from the model bridge calculations and that from the real bridge calculations is in the same order of magnitude. It is to be noted that the calculations for the FOS based on the model bridge include both single and double loads applied at the midspan and close to the interface (P1M, P1J, P2M and P2J), whereas, those based on the real bridge include only the typical load case of a single load at midspan (P1M). The overall factor of safety is calculated in **Table 12** and is approximately equal to 3.5.

Table 12 –Average factor of safety against the design wheel load

Factor of safety	1:2 scaled model bridge			Real bridge		Average FOS
	Test	FEA	CSCT	CSCT	FEA	
Load cases considered	14	14	14	2	2	
Average value	3.05	2.96	3.31	3.98	3.83	≈ 3.5

SUMMARY AND CONCLUSIONS

Based on the experimental, numerical and theoretical analyses, following important conclusions have been drawn:

- All the tests showed failure in punching shear. Failure always occurred in the span of the slab regardless of the number and position of the loads. The interface between the girders and the deck slab was also safe. The combined effect of an increasing transverse prestressing level and compressive membrane action enhanced the bearing (punching shear) capacity.

- Eurocode 2 and ACI 318 give conservative results since they consider a very low contribution of the in-plane forces leading to the conclusion that compressive membrane action should be considered at least for the assessment of old bridges.

- For the real bridge, an overall factor of safety of about 3.5 is obtained against the design wheel load. Such a high safety margin is due to the beneficial effect of compressive membrane action that gives a reserve capacity for old bridges.

- The theoretical analyses based on the CSCT shows that the mechanical model satisfies the experimental results fairly well. The modified level of approximation approach is found to give satisfactory results. The model also seems to simulate the size effect properly in its equations.

- For most cases, an elementary LoA (or Level II LoA from MC2010) using CSCT can serve as a quick assessment of the punching shear capacity.

- The advanced LoA results prove the effectiveness of considering compressive membrane action in the load-rotation behavior of a structure.

- The advanced LoA approach involving compressive membrane action can also be used for laterally restrained reinforced concrete slabs or deck slabs.

ACKNOWLEDGMENTS

The authors wish to express their gratitude and sincere appreciation to Rijkswaterstaat, Ministry of Infrastructure and the Environment, the Netherlands for funding the experimental program. The authors are also grateful to the University of Engineering and Technology Lahore, Pakistan, and SOOB (Stichting Stimulering Onderwijs en Onderzoek Betonconstructies), the Netherlands for additional financial support during the course of this research.

REFERENCES

1. EN 1992-1-1:2005, "*Eurocode 2—Design of Concrete Structures: Part 1-1. General Rules and Rules for Buildings*," Comité Européen de Normalisation (CEN), Brussels, Belgium, 2005, 229 pp.

2. Amir, S.; van der Veen, C.; Walraven, J. C.; de Boer, A., "Experiments on Punching Shear Behavior of Prestressed Concrete Bridge Decks," *ACI Structural Journal*, Volume 113 (3), 2016, pp. 627-636.

3. Amir, S.; van der Veen, C.; Walraven, J. C.; de Boer, A., "Punching Shear in Prestressed Concrete Deck Slabs: Parametric Study," *ACI Structural Journal*, Volume 116 (4), 2019, pp. 169-181.

4. DIANA. FX+. (2012). User's Manual 9.4.4. Delft: TNO Building and Construction Research.

5. Amir, S., "*Compressive Membrane Action in Prestressed Concrete Deck Slabs*," PhD thesis, Delft University of Technology, Delft, the Netherlands, June 2014, 282 pp.

6. Amir, S.; van der Veen, C.; Walraven, J. C.; de Boer, A., "Numerical investigation of the punching shear capacity of transversely prestressed concrete deck slabs," *Structural Concrete*, Volume 20 (3), 2019, pp. 1109-1122. https://doi.org/10.1002/suco.201800285.

7. Amir, S.; van der Veen, C.; Walraven, J. C.; de Boer, A., "Numerical investigation of the bearing capacity of transversely prestressed concrete deck slabs," Computational Modelling of Concrete and concrete Structures, *Proceedings of the EURO-C 2014, St. Anton am Arlberg*, Austria, Taylor & Francis Group, London, ISBN 978-1-138-00145-9, March 2014, pp. 999-1009.

8. Amir, S.; van der Veen, C.; Walraven, J. C.; de Boer, A., "Experimental and numerical investigation of the effect of size in post-tensioned concrete deck slabs," *Proceedings of the Third European and Mediterranean Structural Engineering and Construction Conference*, Limassol, Cyprus, August 3-8, 2020.

9. Model Code 2010, *Final Draft Volume I and* II, Bulletin 65 and 66, *fib* 2012.

10. EN 1991-2:2002, "*Eurocode 1 – Actions on Structures - Part 2: Traffic loads on bridges*," Comité Européen de Normalisation (CEN), Brussels, Belgium, 2002, 168 pp.

11. Hewitt, B.E.; Batchelor, B deV., "Punching shear strength of restrained slabs," *Journal of the Structural Division*, ASCE, Volume 101 (9), pp. 1837-1853.

12. Hon, A.; Taplin, G.; Al-Mahaidi, R. S., "Strength of reinforced concrete bridge decks under compressive membrane action," *ACI Structural Journal*, Volume 102 (3), 2005, pp. 393-401.

13. Kirkpatrick, J.; Rankin, G. I. B.; Long, A. E., "Strength evaluation of M-beam bridge deck slabs, Structural Engineer," Volume 62b (3), 1984, pp. 60-68.

14. Batchelor, B. de V., "Membrane Enhancement in Top Slabs of Concrete Bridges," *Concrete Bridge Engineering*, Performance and advances, 1990, pp. 189-213.

15. Bakht, B.; Jaeger, L. G., "Ultimate load test of slab-on-girder bridge," *Journal of Structural Engineering*, ASCE, Volume 118 (6), 1992, pp. 1608-1624.

16. Mufti, A. A.; Jaeger, L. G.; Bakht, B; Wegner, L.D., "Experimental investigation of fibre reinforced concrete deck slabs without internal steel reinforcement," *Canadian Journal of Civil Engineering*, Volume 20 (3), 1993, pp. 398-406.

17. Fang, I. K.; Lee, J. H.; Chen, C. R., "Behavior of partially restrained slabs under concentrated load," *ACI Structural Journal*, Volume 91 (2), 1994, pp. 133-139.

18. OHBDC, *Ontario Highway Bridge Design Code*, 3rd edition, Ontario Ministry of Transportation (MTO), Highway Engineering Division, Ontario, Canada, 1991.

19. UK Highways Agency BD 81/02, "Use of Compressive Membrane Action in bridge decks," *Design Manual for Roads and Bridges*, Volume 3, Section 4, part 20, 2002, 20 pp.

20. He, W., "*Punching behaviour of composite bridge decks with transverse prestre*ssing," PhD thesis, Queen's University, Kingston, Ontario, Canada, 1992, 228 pp.

21. Amir, S.; van der Veen, C., "*Bearing capacity of transversely prestressed concrete decks*," Stevin Report No. 25.5.13-06, Delft University of Technology, the Netherlands, 2013, 243 pp.

22. RTD 1016:2012, "Guidelines for nonlinear finite element analysis of concrete structures," *Rijkswaterstaat Technisch Document (RTD)*, 2012.

23. Hordijk, D. A., "*Local Approach to Fatigue of Concrete*," PhD thesis, Delft University of Technology, the Netherlands, 1991.

24. Bazant, Z. P.; Cao, Z., "Size effect in punching shear failure of slabs," *ACI Structural Journal*, Volume 84, 1987, pp. 44-53.

25. Regan, P. E., "Behavior of reinforced concrete flat slabs," *CIRIA Report No.89*, Construction Industry Research and Information Association, London, UK, 1981, 89 pp.

26. Walraven, J. C., *Background report 25.5-02-37-prENV 1992-1-1:2002*, Section 6.4, Delft University of Technology, the Netherlands, 2002.

27. ACI Committee 318, "Building Code Requirements for Structural Concrete (ACI 318-19) and Commentary (ACI 318R-19)," *American Concrete Institute*, Farmington Hills, Michigan, USA, 2019.

28. Muttoni, A., "Punching shear strength of reinforced concrete slabs without transverse reinforcement," *ACI Structural Journal*, Volume 105 (4), 2008, pp. 440-450.

29. Clément, T.; Ramos, A. P.; Fernández Ruiz, M.; and Muttoni, A., "Design for punching of prestressed concrete slabs," *Structural Concrete*, Volume 14, 2013, pp. 157-167.

30. Muttoni, A.; Fernández Ruiz, M., "The levels-of-approximation approach in MC 2010: application to punching shear provisions," *Structural Concrete*, Volume 13, 2012, pp. 32-41.

31. Muttoni, A.; Fernández Ruiz, M., "Levels-of-Approximation Approach in Codes of Practice," *Structural Engineering International*, Volume 22 (2), 2012, pp. 190-194.

32. Mitchell, D.; Cook, W. D.; Dilger, W., "Effects of size, geometry and material properties on punching shear resistance," *Punching Shear in Reinforced Concrete Slabs, ACI SP-232-3*, 2005, pp. 39-56.

33. Cervenka, C., "Reliability-based non-linear analysis according to fib Model Code 2010," *Structural Concrete*, Volume 14 (1), 2012, pp. 19-28.

34. RTD 1006:2013, RBK, "Richtlijnen Beoordeling Kunstwerken," *Rijkswaterstaat Technisch Document (RTD)*, 2013.

35. EN 1990+A1+A1/C2:2011/NB:2011, "National Annex to EN 1990+A1+A1/C2: *Eurocode: Basis of structural design*, 2011, 37 pp.

36. Amir, S.; van der Veen, C.; Walraven, J. C.; de Boer, A., "Punching shear capacity of bridge decks regarding compressive membrane action," *HERON, Special issue: Shear in Concrete*, Volume 60 (3), 2015, pp. 235-256.

Biography

Sana Amir is an Assistant Professor of Civil Engineering at the University of Wollongong in Dubai, UAE. She received her PhD in Civil Engineering from Delft University of Technology, the Netherlands. Her research interests include green concrete, sustainable bridge solutions, compressive membrane action, punching shear and finite element analysis. Email: sanaamir.1919@gmail.com.

Cor van der Veen is an emeritus Professor at Delft University of Technology, the Netherlands, where he received his MSc and PhD in Civil Engineering. His research interests include very-high-strength steel-fiber concrete, concrete bridges, and computational mechanics.

Joost Walraven is emeritus Professor at Delft University of Technology, the Netherlands, where he received his MSc and PhD in Civil Engineering. His research interests include the development of advanced models for the behavior of concrete structures and new types of concrete. He was convenor of the Project Team for Eurocode 2 "Concrete Structures" and for the *fib* Model Code for Concrete Structures 2010.

Ane de Boer is now a Consultant and was formerly Specialist Bridges and Viadcuts at the Ministry of Infrastructure and the Environment. He got his MSc and PhD at Delft University of Technology. His research interest are existing structures, traffic flows and its belonging weights and computational mechanics.